sustainability

MDPI

Article

Effect of Rebar Harsh Storage Conditions on the Flexural Behavior of Glass FRP Concrete

Sami W. Tabsh [1,*], Adil Tamimi [1], Magdi El-Emam [1] and Ali Zandavi [2]

[1] Department of Civil Engineering, College of Engineering, The American University of Sharjah, Sharjah P.O. Box 26666, United Arab Emirates; atamimi@aus.edu (A.T.); melemam@aus.edu (M.E.-E.)
[2] Qeyas Contracting L.L.C., Dubai P.O. Box 74956, United Arab Emirates; asayed@qeyascontracting.ae
* Correspondence: stabsh@aus.edu

Abstract: Nowadays, fiber-reinforced polymer (FRP) has become a widely accepted alternative reinforcement to steel bars in concrete members due to its many sustainability traits, as represented by its high strength-to-weight ratio, corrosion resistance, non-conductive properties, and electromagnet neutrality. However, FRP bar exposure for an extended period of time to harsh environmental conditions and chemicals can have an adverse effect on their mechanical properties. In this investigation, glass FRP bars were exposed to indoor controlled temperature, outdoor direct sunlight, outdoor shade, seawater, and alkaline solution for six months prior to using them as reinforcement in concrete flexural members. This research involves the fabrication and testing of five pairs of 3 m-long concrete beams with 200 mm by 300 mm cross-sections embedded in the tension zone with the exposed GFRP bars. The 10 beams were instrumented with strain gauges and tested following a four-point loading scheme using a hydraulic jack attached to a rigid steel frame. Crack width records from the tests showed the inferior serviceability of the beams that contained rebars stored in an outdoor environment relative to the control beams. GFRP bar exposure to an alkaline solution or outdoor direct sunlight slightly affected the cracking and ultimate moment capacities, reducing them by 5% and 3% in terms of the same parameters as the controlled indoor exposure, respectively. The influence of GFRP bar exposure to open-air shade or sunlight decreased the pre-cracking stiffness by 25% and flexural ductility by 10–20% when compared with the control specimens. The predicted ultimate flexural strength using the ACI 440 provisions gave comparable results to the experimentally obtained values. A simple mathematical equation that envelops the moment–deflection relationship for GFRP over-reinforced concrete beams and only requires information about initial cracking and ultimate flexural conditions is proposed.

Keywords: composites; environmental exposure; flexure; glass-fiber-reinforced polymer; reinforced concrete; sustainability

Citation: Tabsh, S.W.; Tamimi, A.; El-Emam, M.; Zandavi, A. Effect of Rebar Harsh Storage Conditions on the Flexural Behavior of Glass FRP Concrete. *Sustainability* **2024**, *16*, 1944. https://doi.org/10.3390/su16051944

Academic Editor: Junsheng Su

Received: 15 January 2024
Revised: 4 February 2024
Accepted: 19 February 2024
Published: 27 February 2024

1. Introduction

The construction industry around the world depends heavily on the use of concrete because its constituents are readily available almost anywhere on Earth. In the past, this material regularly utilized steel reinforcement in the form of rebars internally placed within the structure to compensate for the weakness of concrete in tension. As a building material, steel-reinforced concrete is strong, functional, adjustable, flexible, durable, and relatively inexpensive. Despite its many benefits, reinforced concrete has some shortcomings that can develop over time, including its susceptibility to delamination, spalling, excessive cracking, and disintegration. All of these aforementioned actions can cause the steel reinforcing bars inside the concrete to rust as a result of electrolysis, a process in which water and chloride ions infiltrate the concrete, resulting in the breakdown of the reinforcement over time due to corrosion. The degradation mechanism of reinforced concrete beams subjected to sustained loading and multi-environmental factors that include gas and liquid corrosive substances, acidic corrosive substances, acid–salt mist, carbon dioxide, and periodic changes in temperature and humidity have been addressed by Li et al. [1].

To prolong the life of reinforced concrete structures and make them more sustainable, one needs to address, among other things, the corrosion problem of steel reinforcement. One solution is to replace the steel with an appropriate high-tensile-strength material that has a minimal potential for deterioration with time, such as fiber-reinforced polymer (FRP). A great benefit of the FRP material is its low potential for corrosion in humid or saline environments because the matrix coating can shield the fibers from direct exposure to moisture, aqueous solutions, or alkaline conditions. In addition, the different types of FRP provide other advantages, such as high strength-to-weight ratios, ease of handling in the field, and insulation from electrical and magnetic fields. The minimum resource use, low environmental impact, and high performance of FRP make this material an ideal contributor to sustainable construction. The most commonly considered types of FRP for structural applications involving concrete are manufactured from carbon, basalt, and glass, all of which offer a greater tensile strength than steel. Glass-fiber-reinforced polymer (GFRP) rebars are particularly desirable because, with all their sustainability traits, they have similar carbon emission factors to steel [2]. A comprehensive review of FRP bars for anticipated use in the next generation of construction projects was compiled by Ji et al. [3].

Although experience has demonstrated that FRP is a more sustainable material than steel due to its higher resistance to corrosion, its mechanical properties can still be negatively impacted by high temperatures, salt water, and chemical solutions. The extended exposure to such harsh environmental settings can be the result of either their storage conditions prior to placement in concrete or contributing factors after incorporation into concrete. The first scenario could involve leaving the FRP rebars for some time in an outdoor environment before utilizing them in construction. The second scenario could be the result of unintended exposure to some chemicals during concrete casting. There are many environmental conditions that contribute to the latter scenario, such as a high pH level while casting due to presence of calcium in the fresh concrete.

Commercially, there are different types of glass fibers that are available for reinforcing a concrete structure, including E-glass, S-glass, C-glass, and AR-glass. In general, such an FRP is characterized by a high strength, good resistance to water and chemicals, and low relative cost. E-glass is the most economical and useful type of glass fiber for construction because of its great resistance to acids and relatively high modulus of elasticity. S-glass tends to have a greater stiffness level than E-glass, but it costs more. C-glass has a useful property, which is chemical stability in harsh environments. AR-glass is suitable for alkaline environments since other types of glass fibers are negatively affected by such conditions.

A large number of past studies have addressed the flexural behavior of concrete beams that are reinforced with glass FRP rebars, sheets, or laminates, as demonstrated in the next section of this paper: the literature review. However, very few investigations have been conducted to understand the effects of exposing bare GFRP bars to harsh environmental conditions on the response of the concrete beams containing them. The significance of this issue is that when the bars are bare, they can be easily affected by direct severe environmental exposure, compared to when they are protected by concrete. Although there are no statistics available on the frequent storage problems of construction materials in practical applications, some professional organizations, such as the Concrete Reinforcing Steel Institute (CRSI), have addressed this issue by providing tips on how to store reinforcement on site properly. For situations in which GFRP bars are not stored properly prior to incorporation during construction, the possible degradation of the material could take place, especially if it was exposed to severe environmental conditions.

This study fills the gap in this regard by presenting the results of an experimental investigation carried out on ten concrete beams reinforced with E-Glass FRP bars that were previously exposed to different environmental conditions for a 6-month duration. The environmental conditions are (1) indoor, (2) unshaded outdoor, (3) shaded outdoor,

(4) alkaline solution, and (5) seawater. Extensive details about the beam specimen size, materials, test setup, and instrumentations are provided later in the paper.

2. Literature Review

While there is a wealth of published research on the structural behavior of concrete beams reinforced with glass-fiber-reinforced polymers, few studies have addressed the influence of the exposure condition of the rebars prior to using them in concrete structures subjected to loads.

With regard to research on bare GFRP rebars, a wealth of research is available in the literature, including a comprehensive review study on its suitability as reinforcement in flexural concrete members [4]. In an early study, Kim et al. [5] determined that the tensile properties of the GFRP rods were significantly reduced under moisture, chloride, alkali, and freeze–thaw cycling conditions. Susceptibility to moisture and alkaline solution greatly affected the degradation of glass fiber, the surrounding matrix, and the interface between the fiber and the matrix. Thereafter, Al-Salloum et al. [6] studied the effect of exposure to harsh environmental conditions for 6, 12, and 18 months on the tensile properties of GFRP bars. At maximum exposure, the test results revealed that at 50 degree Celsius the tap water and alkaline solution had the maximum detrimental impact on the tensile strength of the tested GFRP bars. In a review paper, Hassan and El Maaddawy [7] found out that the limits on sustained loading for aggressive environments by codes were outdated, the conditioning of fiber glass in alkaline solutions was more critical than in concrete, and an increase in moisture uptake had a minor effect on the mechanical properties. Manalo et al. [8] assessed the physical, mechanical, and microstructural properties of GFRP bars subjected to severe moisture, saline, and alkaline conditions. The results showed that the alkaline solution was more critical to the GFRP bars than tap water or saline solution, resulting in damage to the fibers, matrix, and chemical composition. Vizentin et al. [9] investigated the long-term effects of sea water environmental conditions on the mechanical properties of FRP used in marine structures. They found out that the exposed FRP coupons exhibited mass increase due to water absorption and growth of algae and micro-organisms, which impacted the tensile strength and surface morphology. Voids were also produced in the matrix material structure due to the extended presence of sea water. The findings of a study by Fergani et al. [10] demonstrated that extreme temperatures can start and speed up the initiation of degradation processes. The long-term mechanical properties of GFRP bars were mainly impacted by moisture diffusion amongst the resin rich layer and debonding at the fiber–matrix interfaces as a result of the dissolution of the silane coupling agents.

Additional research on exposed GFRP rebars includes the work of Davalos et al. [11] who found out that moisture and elevated temperature were more critical to the durability degradation of GFRP bars than alkalinity and low sustained load. The degradation rate of the tensile strength of GFRP bars in saturated concrete subjected to a sustained load kept decreasing rapidly, while it converged to a constant value with the increase in exposure time when subjected to a high temperature. Gooranorimi and Nanni [12] investigated the performance of GFRP bars exposed to concrete alkalinity and ambient conditions in an old bridge. The test findings did not show any indication of GFRP microstructural damage or alteration of chemical properties, and the fiber contents were comparable to new values, while the horizontal shear strength values were inconclusive. Arczewska et al. [13] concluded that the immersion of GFRP bars in a high-pH alkaline solution decreased the strength of the bars, and the rate of strength deterioration was affected by the temperature of the solution. Bent bars deteriorated faster than straight bars, smaller diameter bars worsened more quickly than larger diameter bars, and bars under a flexural effect within the tension zone weakened sooner than those under direct tension. Jin et al. [14] concluded that the tensile strength of GFRP bars subjected to an alkaline solution degraded faster under a high stress level than under low stress level. On the other hand, the elastic modulus and Poisson’s ratio of the bars increased at first but then decreased with the increase in loading and immersion time. Al-Tamimi et al. [15] showed that there was a negligible difference in bond stress between 60 and 90 days of exposure both under direct sunlight and cyclic sea water splashing, with the main failure mode in the pullout tests being pure slippage. Lu et al. [16] demonstrated that the failure mode of fiber rupture in the tensile test and horizontal cracking in the short-beam shear test did not significantly alter with the increase in the exposure period. Nevertheless, the influence of immersion solutions on the deterioration in durability properties occurred in the ultimate strength and corresponding strain at failure.

Concerning studies on the structural behavior of concrete beams that are reinforced with GRFP bars, plenty of research exists on the subject. For example, Maranan et al. [17] found out that the size of the reinforcement had a negligible impact on the performance, serviceability was improved with an increase in the reinforcement ratio, sand coating on rebars can provide a sufficient bond between the reinforcement and concrete, and current code provisions under-estimate the flexural strength of GFRP-reinforced geopolymer concrete. Nematzadeh and Fallah-Valukolaee [18] demonstrated an improvement in the flexural strength, stiffness, and ductility of concrete beams that were reinforced with both steel and GFRP rebars. A proposed analytical model for the flexural response was able to predict by sectional analysis the ultimate strength and deflection. Abbas et al. [19] explored the effect of changing the proportion and configuration of steel and GFRP rebars on the flexural performance of under-reinforced concrete beams. The findings of the investigation showed that serviceability and ductility can be greatly improved with the increase in the steel area. The incorporation of steel fibers in concrete enhanced the flexural serviceability in terms of the cracking moment and elastic stiffness. Research by Muhammad and Ahmed [20] on the flexural behavior of reinforced concrete beams containing GFRP bars exhibited a higher strength, lower deflection, and smaller crack width for the beams employing high-strength concrete over those utilizing normal strength concrete. Mohammed et al. [21] concluded that the addition of PET fibers to GFRP-reinforced concrete beams decreased the cracking and ultimate moments and their corresponding deflections, but had an insignificant impact on the ductility, crack propagation, and failure mode. Also, the serviceability of the beams increased by up to 12% and flexural stiffness by 25% with the use of PET waste fiber.

Other studies on structural performance of GFRP-reinforced concrete beams include the work of Elangovan and Rajanandhini [22] who researched the flexural behavior of GFRP concrete beam containing M-sand, a by-product of quarrying and breaking of blue metal. The findings of the study showed that concrete beams containing M-sand and reinforced with GFRP possessed a 12% higher load than corresponding beams with river sand and reinforced with steel, although the lower modulus of elasticity of the GFRP bars affected the post-cracking stiffness. Farias et al. [23] compared the flexural behavior of GFRP-reinforced concrete beams with corresponding concrete beams containing a steel area equal to 40% of the fiber glass area. The results of the study showed that the beams with GFRP bars possessed a 64% higher flexural resistance and exhibited less deflection compared with those containing steel bars. Shawki Ali et al. [24] found that the beams with carbon-fiber-reinforced polymers (CFRP) bars could withstand a higher load and absorb more fracture energy than steel. With more reinforcement, CFRP showed a greater load-carrying capacity than GFRP due to its higher tensile strength and modulus of elasticity. Results from Gouda et al. [25] confirmed the enhancement in ductility and ultimate capacity of concrete beams that were reinforced with ribbed GFRP bars due to the increase in the confinement in the bending zone by closely spaced stirrups. Moreover, GFRP-reinforced concrete beams with a low reinforcement ratio demonstrated a bilinear load–deflection behavior, whereas corresponding beams with a higher reinforcement ratio exhibited a trilinear response. Hassan et al. [26] studied the structural performance of concrete beams internally reinforced by GFRP bars and externally strengthened by CFRP sheets. The results of the investigation showed that the use of twin-layer CFRP sheets can increase the flexural strength of beams containing minimum GFRP reinforcement by 95% over the control beam that was not strengthened, leading to a change in the mode of failure from GFRP bars' rupture to concrete crushing.

3. Experimental Program

The objective of the research study was to investigate the effect of the long-term storage conditions of bare GFRP rebars on the flexural behavior of concrete beams utilizing such reinforcement. To achieve this goal, an experimental program was designed that included five pairs of 3000 mm-long beams with a 200 mm by 300 mm rectangular cross-section. The beams were reinforced with two No. 12 GFRP bars at the bottom and No. 10 closed stirrups at 100 mm spacing along the entire length specimens. The stirrups were designed so that potential shear failure near the supports would not take place. Two No. 10 steel bars were placed at the top in order to secure the stirrups into their intended locations. The test setup of the beams consisted of a 4-point loading scheme with a simple span between supports equal to 2700 mm and 150 mm overhangs from both ends beyond the supports. The distance between the applied two loads within the central region of the beam was equal to 600 mm, resulting in a 1050 mm shear span on both sides of the applied loads, as shown in Figure 1.

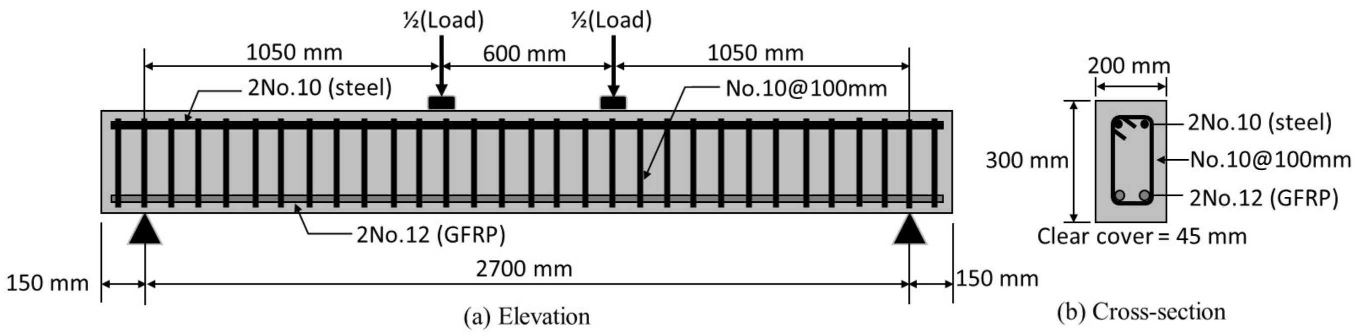

Figure 1. Details of the beams considered in the experimental program.

The beam specimens were supported on two rollers that were mounted on large concrete pedestals laid on a hard floor. They were loaded from the top by a hydraulic jack fixed to a rigid steel portal frame. The load from the jack was divided into two equal forces on top of the beam by a rigid structural steel member, with a load cell being inserted between the jack and the rigid member. Five 60 mm-long strain gauges were placed horizontally at equal distances on one the side of the beam at midspan, starting 30 mm from the top, to measure longitudinal deformation in the concrete due to flexure. Two 10 mm-long strain gauges were installed on the surface of each of the two GFRP bars within the flexure-critical central region of the beam. A data acquisition system was used to store the recorded data from the jack, load cell, and strain gauges throughout the test. The details of the experimental test setup and instrumentation are presented in Figure 2.

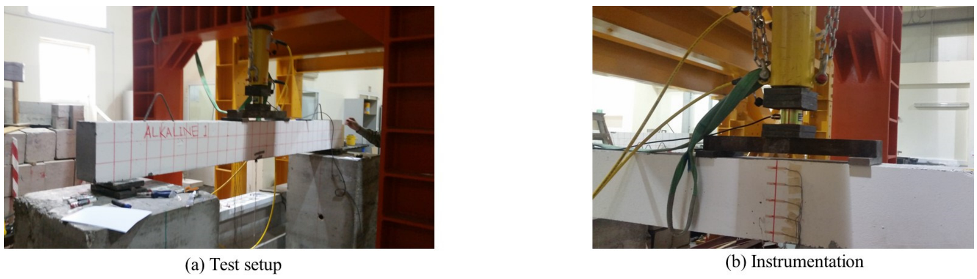

Figure 2. Details of the experimental test setup and instrumentation.

Prior to using the GFRP bars within the concrete beams, they were subjected to five different exposure settings: (1) indoor controlled climate, (2) outdoor under direct sun light, (3) outdoor in the shade, (4) alkaline solution containing a high pH level, and (5) circulated seawater in a tank, as shown in Table 1 and Figure 3. The duration of the exposure was for about 6 months, from June 10 to December 20 of the same year. The time of exposure coincided with the hot summer season of the country where the research was conducted.

Table 1. Beams considered in the study and their corresponding exposure.

Beams Label	Exposure Condition
Lab 1 and Lab 2	Indoor controlled climate at 22–25 °C
Sun 1 and Sun 2	Outdoor direct sun light (9–48 °C)
Shade 1 and Shade 2	Outdoor in the shade (9–48 °C)
Alkaline 1 and Alkaline 2	Solution having pH value of 12.99 pH
Salt 1 and Salt 2	Salinity between 38 and 41 g/kg

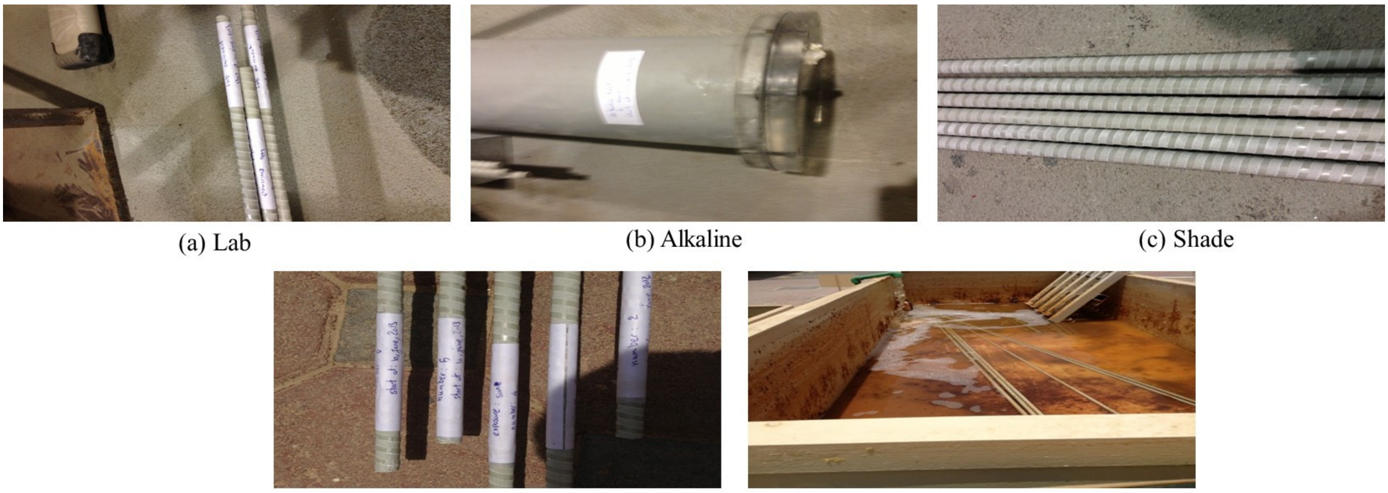

(a) Lab (b) Alkaline (c) Shade

(d) Sun (e) Salt

Figure 3. Exposure of GFRP rebars prior to using them in concrete beams.

For the bars that were kept indoors under a controlled climate, the temperature resulting from the air-conditioned setting varied within a narrow range, 22–25 °C. The bars that were placed outdoor in the city of Sharjah, UAE, experienced very dry, hot and humid climate conditions from June to September, and warm and dry climate conditions from October to December. Weather records during the exposure period showed temperatures as high as 48 °C and as low as 9 °C. The average monthly highest temperature, lowest temperature, and range of wind speed during the exposure period of the bars are presented in Table 2. No precipitation was observed during the outdoor exposure period, which is common in this arid region of the world. For the bars that were exposed to an alkaline solution, the bars were kept inside a closed pipe filled with a high-alkaline solution of which the pH value was 12.99 pH. In the fifth scenario, the GFRP bars were kept in a large water tank filled with circulating seawater with the help of a pump. In this study, the seawater was brought from the Arbian Gulf, which has a salinity level that varies between 38 and 41 g/kg at the surface of the water during the year.

Table 2. Average monthly weather condition for the outdoor GFRP bars.

Weather Condition	June	July	August	September	October	November	December
Maximum Temperature (°C)	35–43	39–48	38–44	35–43	32–40	25–37	19–31
Minimum Temperature (°C)	23–30	29–34	29–34	25–31	21–27	17–24	9–20
Range of Wind Speed (km/h)	0–29	0–35	0–45	0–48	0–29	0–37	0–35

Following exposure of the GFRP bars to the different environmental conditions, the stirrups were fabricated, reinforcement cages were assembled, and GFRP bars were equipped with strain gauges and placed inside the plywood formwork. Concrete work was later carried out on the beams, as shown in Figure 4. Note that 10 beams were constructed, of which a pair of two beams was fabricated the same way in order to check the variation in the outcome of the tests.

(a) Formwork (b) Strengthening of formwork (c) Casted concrete

Figure 4. Fabrication of the beams used in the study.

4. Materials and Methods

The GFRP bars employed in the study were fabricated by pultrusion using E-glass fibers and thermoplastic resin. The surface of the reinforcement was composed of an indented, ribbed surface that is cut into hardened bars. Manufactured composite reinforcing bars containing thermoplastic resin show strength and elasticity properties analogous to those of thermoset materials containing a corresponding amount of fibers of identical type. Three 12 mm-diameter and 300 mm-long GFRP bar samples were tested in tension using a universal test machine at a loading rate of 2 mm/minute. The average tensile strength of the GFRP bars was 950 MPa and the elastic modulus of elasticity was 40.8 GPa. As expected, all tests showed elastic behavior up to reaching the tensile strength, without any post-peak residual response.

The No. 10 steel reinforcement that was used as top hanger bars for the stirrups in the beams was based on the UK-BS4449 2005 specification with a grade B500B or 500 MPa characteristic (nominal) yield strength. The average measured mechanical properties from the tension tests of three specimens gave a 200 GPa modulus of elasticity, 570 MPa yield stress, and 700 MPa ultimate tensile stress.

Ready-mix concrete with a target cube strength at 28 days equal to 50 MPa was ordered from a local supplier. The concrete mix had a water–cement ratio equal to 0.34 and mass density of 2470 kg/m^3. It was characterized by its high flowability that helped during concrete casting with minimal vibration effort. The concrete mix proportions of the constituents per 1.0 m^3 of concrete are presented in Table 3. The average 150 mm cube strengths at the age of 7, 14, and 28 days from casting were, respectively, 41.3, 43.7, and 48.1 MPa. The corresponding average 150 mm by 300 mm cylinder strengths at the age of 7, 14, and 28 days from casting were, respectively, 24.4, 33.4, and 38.4 MPa. For predicting the nominal flexural characteristics of the beams by theory following the procedures contained in relevant design codes, the concrete cylinder compressive strength of 38.4 MPa was used. Figure 5 shows the tested concrete, GFRP, and steel materials used in the research study.

The 10 constructed beams were wet cured after concrete casting and hardening by daily dousing the blanketed surface of the specimens with water for a period of two weeks. They were then painted white and 100 mm by 100 mm grid lines were drawn on one side surface of the beams to identify and track the location and extension of cracks during testing. They were tested by a 4-point test setup over a period of 4 days under a displacement-controlled loading environment. All beams exhibited a flexural mode of failure through mainly vertical cracks that were concentrated within the middle region, where the maximum bending moment occurred. As intended, no major diagonal tension cracks formed within the shear-critical side regions of the beams throughout the tests; hence, the results represent flexural behavior. Figure 6 shows 5 of the 10 tested beams being loaded during the laboratory experiments.

Table 3. Concrete mix design proportions.

Constituents	Amount (kg per m^3 of Concrete)
Ordinary Portland Cement	425
Microsilica	25
Water	151
Crushed Washed Sand	290
Red Dune Sand	390
Coarse Aggregate (Maximum size = 20 mm)	1180
Additives (MegaFlow 2000 and MegaddVE)	9

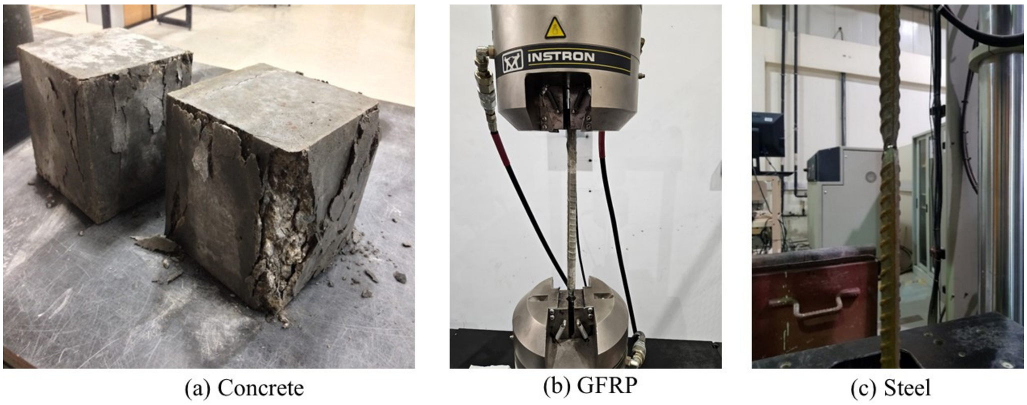

Figure 5. Testing of concrete, GFRP and steel material.

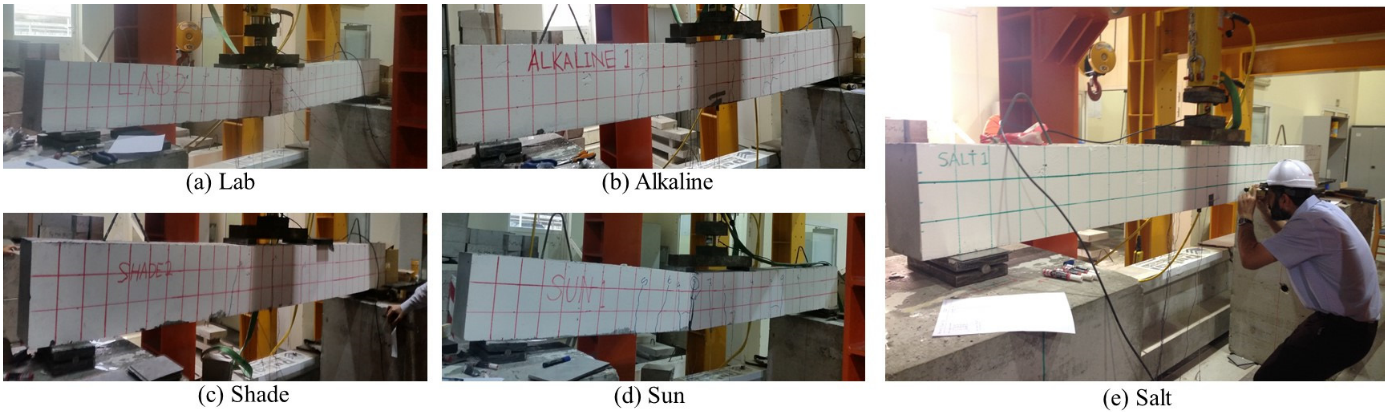

Figure 6. Experimental testing of 5 of the 10 beams that were considered in the study.

5. Results

In this section, the raw data obtained from the experiments are organized and analyzed in order to determine the influence of the storage exposure conditions of GFRP rebars on the flexural behavior of the concrete beams containing them. Also included are two subsections that address the theoretical prediction of the structural response using equations included in the relevant structural design codes.

5.1. Analysis of Experimental Findings

Four-point testing of beams provides a convenient way of studying the behavior of structural members subjected to flexure since the middle region is subjected to pure flexure. For the successful implementation of such a testing scheme, the beam must be strengthened against shear failure within the two zones that extend between the reaction and near load.

In this study, the load–deflection curves of every pair of beams for which the GFRP bar reinforcement was subjected to the same exposure condition were plotted on the same graph, as shown in Figure 7. Note that the load shown in the figure is the total combined load applied by the jack at the two locations within the central region of the beam. The records of the test results showed that the flexural responses of every pair of beams were similar, thus indicating proper beam fabrication and testing procedures. As expected, the variation in the cracking load for similar beams (7.0–33.0%) was much larger than the corresponding variation in the ultimate load (2.4–9.8%) since the cracking moment is mainly a function of the tensile strength of concrete, which possesses a high uncertainty. All of the load–deflection relationships exhibited a two-stage behavior, one prior to concrete cracking and another after initiation of the first crack. The first stage started linearly from the origin up to the load that caused the bottom fibers of the cross-section within the maximum bending moment region to reach the modulus of rupture of the concrete. Thereafter, the load was suddenly reduced until the GFRP bars took over the load from the cracked concrete section. After initial cracking, the flexural stiffness of the beam remarkably reduced with the formation of new cracks and the extension of older ones until failure.

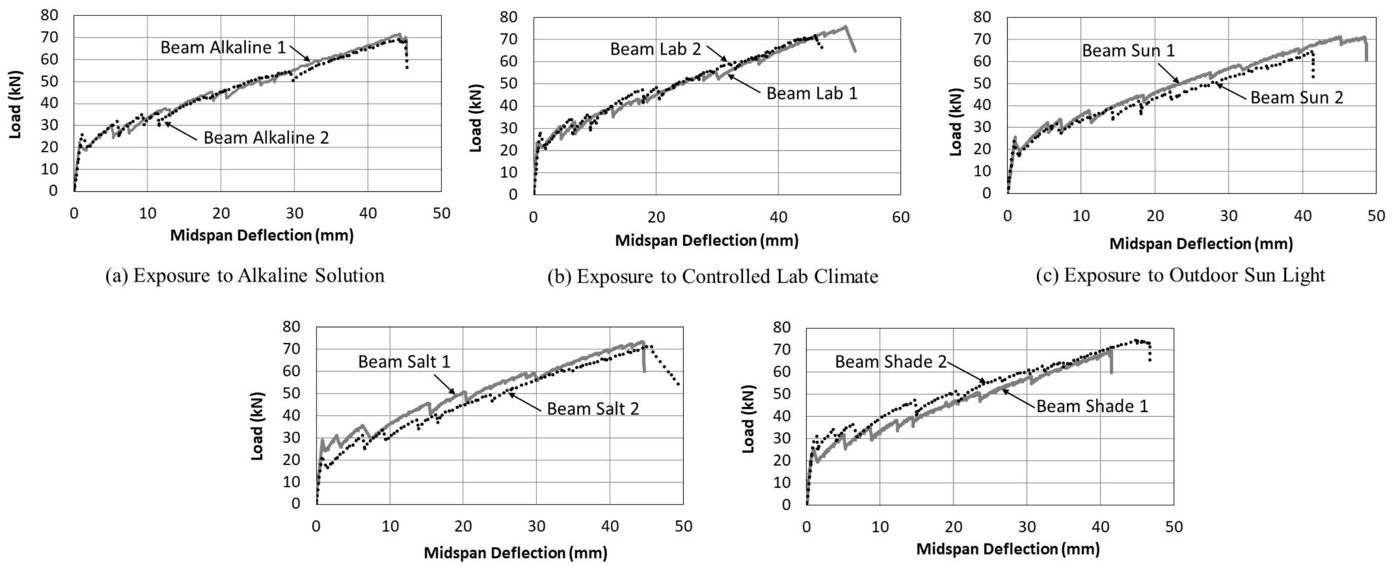

(a) Exposure to Alkaline Solution (b) Exposure to Controlled Lab Climate (c) Exposure to Outdoor Sun Light

(d) Exposure to Seawater (e) Exposure to Outdoor Shade

Figure 7. Experimental load–deflection relationships for the 10 tested beams.

After formation of the initial crack, the load–defection relationship of the beams experienced multiple smaller peaks as a result of additional concrete cracking within the flexural tension zone. Typically, there were 6–9 vertically oriented flexural cracks in a given beam, with one or two major cracks that significantly progressed and opened up as the load was increased. No diagonal tension cracks were observed, even in the high shear regions of the beams near the supports. Figure 8 shows the cracking pattern of the beam Salt 1 just before reaching the ultimate bending moment capacity, which is typical of what was observed in all the beams.

Not all strain gauges that were mounted on the GFRP bars were operable during the entire tests. In addition, the strain gauges that were placed on the concrete side surface of the beams did not give useful data because they did not match the location of the most critical crack. As expected, the working strain gauge records for the GFRP rebars during the tests obtained by the data acquisition system exhibited a nearly linear bevavior, as shown in Figure 9a. This is because the GFRP reinforcement follows a linearly elastic behavior at the material level up to rupture. Information on crack width was obtained and analyzed for the beams as a function of the total applied load. Figure 9b shows data on the most critical flexural crack within the maximum bending moment region for some of the beams. The crack width and propagation results clearly indicated the superior serviceability behavior of the beams that incorporated rebars that were stored in a controlled environment in the laboratory (Lab 1), especially when compared with the beams that included rebars that were previously stored for an extended time outdoors (Shade 1 and Sun 2).

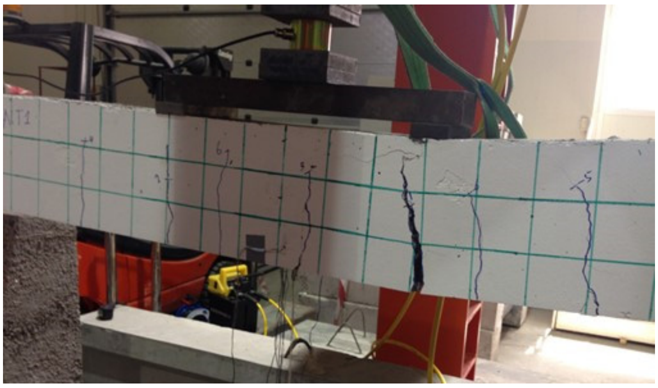

Figure 8. Cracking pattern of the tested beam Salt 1 just before ultimate condition.

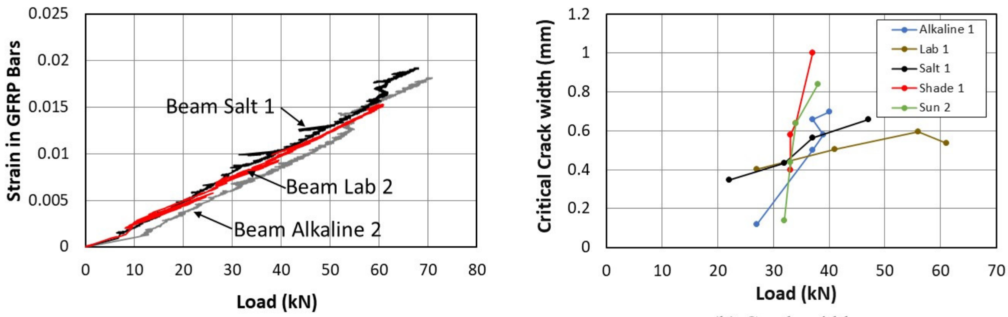

(a) Strain in GFRP bars (b) Crack width

Figure 9. GFRP bars strain gauge and crack width records for some of the tested beams.

The experimental load–deflection interactions were converted into maximum bending moment–deflection relationships by multiplying one-half of the total applied load through the jack by the shear span (1.05 m), defined as the distance between the support reaction and near load. To study the effect of different GFRP bar storage conditions on the flexural behavior of concrete beams embedded with such reinforcement, the bending moment–deflection curves for all beams must be plotted on the same graph. To avoid congesting the load effect versus the deformation diagram due to the closely spaced curves, the responses of only five beams were considered at a time. Figure 10 shows the moment–deflection curves for the five beams that gave a lower flexural capacity at ultimate, the five beams that gave a higher flexural capacity at ultimate, and the corresponding five averages of each pair of curves. Table 4 provides details about the cracking bending moment, pre-cracking flexural stiffness, ultimate bending moment, post-cracking flexural stiffness, ductility, and mode failure for each of the 10 tested beams. The corresponding average parameters for each pair of beams that were subjected to the same bar exposure are given in Table 5.

Careful analysis of the relationships in Figure 10 shows that all three groups of moment–deflection curves had similar overall trends in terms of serviceability, strength, and ductility. The moment capacity of the tested beams at initial cracking and ultimate varied within 11.49–16.42 kN·m, and 34.04–39.93 kN·m, respectively. The flexural strength at ultimate represented approximately 2.4–3.3 times the corresponding flexural cracking strength. On the other hand, the stiffness of the tested beams prior to cracking and after cracking ranged from 11,692 to 19,724 kN·m/m and 508 to 593 kN·m/m, respectively. The flexural pre-cracking stiffness represented roughly 23–33 times the corresponding post-cracking flexural stiffness. Note that the post-cracking stiffness was determined by dividing the difference between the ultimate and cracking moments by the difference in the associated deflection since the slope of the envelope of the moment–deflection curve following cracking was nearly constant. The higher variability observed in pre-cracking stiffness is because it is largely controlled by the tensile strength and modulus of elasticity of the large uncracked concrete section, which are both highly variable. On the other hand, the lower variability depicted in the post-cracking stiffness is because it is dependent on the compressive strength and modulus of elasticity of the small cracked concrete section as well as the modulus of elasticity of the GFRP bars, which was negligibly affected by the environmental exposure, as shown by Abed and ElMesallami [27].

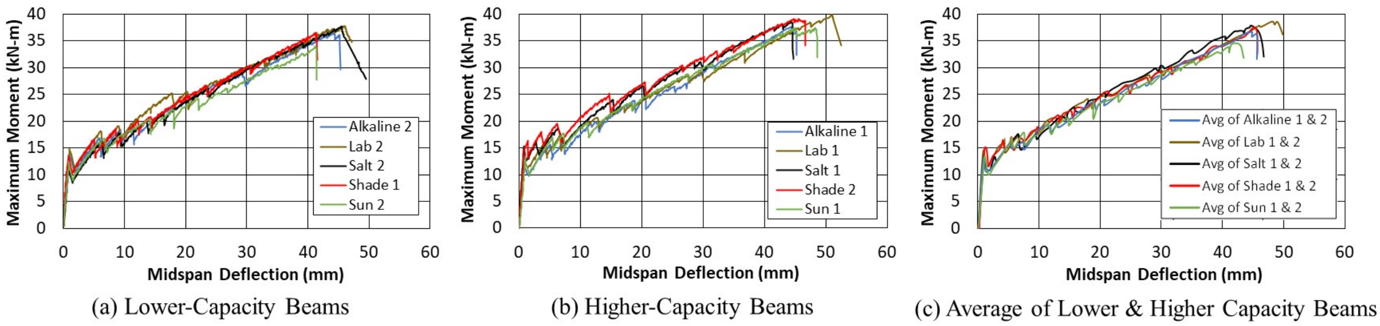

Figure 10. Moment–deflection response for the lower, higher, and average capacity beams.

Table 4. Important flexural parameters of all 10 tested beams.

Flexural Parameter	Alkal. 1	Alkal. 2	Lab 1	Lab 2	Salt 1	Salt 2	Shade 1	Shade 2	Sun 1	Sun 2
Cracking Moment (kN·m)	11.85	13.91	12.26	14.87	15.28	11.49	13.48	16.42	13.45	12.57
Pre-Cracking Stiffness (kN·m/m)	14,484	13,366	19,724	14,899	18,016	15,143	14,460	11,692	12,963	13,556
Ultimate Moment (kN·m)	37.57	36.37	39.93	37.76	38.59	37.70	36.55	39.09	37.40	34.04
Post-Cracking Stiffness (kN·m/m)	593	520	550	508	536	587	569	522	545	534
Ductility Index ($\eta = \Delta_u / \Delta_{cr}$)	3.73	3.18	4.16	3.10	2.90	3.95	3.08	2.73	3.34	3.27
Flexural Mode of Failure [1]	CC	CC	CC	CC	CC	CC	CC	BF	CC	BF

[1] CC = concrete crushing, BF = GFRP bar fracture.

Table 5. Average flexural parameters for each pair of the tested beams.

Average Flexural Parameter	Alkaline	Lab	Salt	Shade	Sun
Cracking Moment (kN·m)	12.88	13.57	13.38	14.95	13.01
Pre-Cracking Stiffness (kN·m/m)	14,107	17,312	16,580	13,076	13,260
Ultimate Moment (kN·m)	36.97	38.84	38.14	37.82	35.72
Post-Cracking Stiffness (kN·m/m)	557	529	562	546	540
Ductility Index ($\eta = \Delta_u / \Delta_{cr}$)	3.45	3.62	3.43	2.90	3.31

Although FRP-reinforced concrete beams generally lack adequate ductility when compared to those that are reinforced with steel bars, beams that are designed to fail by concrete compression are not as brittle as corresponding beams that are designed to fail by FRP-reinforcement rupture. To contrast the relative ductility of the tested beams, we consider the ductility index, η, defined as the ratio of the deflection at ultimate, Δ_u, to that at initial cracking, Δ_{cr}. The results of experimental testing showed that the ductility index of the tested beams varied between 2.73 and 4.15, with the higher values being associated with the indoor bar exposure and lower values associated with the outdoor bar exposure.

As expected, the cracking moment and pre-cracking stiffness were susceptible to large variations due to their high dependence on the modulus of rupture of the concrete, which was highly volatile in nature. The two extreme and average responses for the five considered GRFP reinforcement exposures indicated that bars subjected to controlled indoor (denoted by Lab) or outdoor shade setting gave the best flexural responses, whereas bars subjected to an alkaline solution or outdoor sun setting yielded the worst flexural responses. The structural behavior of the concrete beams under bending that contained GFRP rebars that were previously exposed to salt water appeared to be moderately impacted by the high concentration of dissolved sodium chloride. Eight of the ten tested beams failed in flexure due to concrete crushing within the top compression zone, while the remaining two beams failed unexpectedly by GFRP bar rupture due to tension without warning. Furthermore, based on strain gauge records and visual observation of the crack pattern and propagation on the surfaces of the specimens, there was no indication of bond failure on any of the tested beams. This outcome agrees with the findings from the experimental study conducted by Abed and ElMesalami [27]. Figure 11 shows photos of the typical modes of failure of beams which collapsed due to concrete crushing and GFRP bar fracture.

(a) Concrete crushing failure of beam Sun 1

(b) GFRP bars rupture failure of beam Shade 2

Figure 11. Typical concrete compression and GFRP bar rupture failures.

5.2. Theoretical Predictions

When planning the experiments in this study, the size and number of the GFRP bars was selected such that the flexural behavior was intended to be within the desirable over-reinforced section classification. Following the provisions of the ACI 440's guide on the design and construction of structural concrete members that are reinforced with FRP bars [28], one can use the material properties and section geometry to determine the nominal flexural strength at ultimate. To do so, we start by computing the GFRP reinforcement ratio, ρ_f, using

$$\rho_f = \frac{A_f}{bd} \tag{1}$$

$$=> \rho_f = \frac{2 * 113}{200 * 239} = 0.00473$$

and compare it with the balanced reinforcement ratio, ρ_{fb}:

$$\rho_{fb} = 0.85\beta_1 \left(\frac{f'_c}{f_{fu}}\right)\left(\frac{E_f\varepsilon_{cu}}{E_f\varepsilon_{cu} + f_{fu}}\right) \tag{2}$$

in which b is the width of the section, d is the depth of the tensile reinforcement from the extreme compressive fibers, A_f is the area of the GFRP bars, f'_c is the concrete compressive strength, f_{fu} is the tensile strength of the GFRP, E_f is the modulus of elasticity of the GFRP, ε_{cu} is the strain in extreme compression fibers of the concrete due to flexure at ultimate (taken equal to 0.003), and β_1 is a parameter that relates the depth of the idealized concrete Whitney's stress block to the depth of the neutral axis from the extreme compression fibers:

$$\beta_1 = 0.85 - 0.05\left(\frac{f'_c - 28}{7}\right) \geq 0.65 \tag{3}$$

For $f'_c = 38.4$ MPa,

$$\beta_1 = 0.85 - 0.05\left(\frac{38.4 - 28}{7}\right) = 0.776$$

Hence,

$$\rho_{fb} = 0.85 * 0.776\left(\frac{38.4}{950}\right)\left(\frac{40,800 * 0.003}{40,800 * 0.003 + 950}\right) = 0.00304$$

which is less than ρ_f; hence, the section is confirmed as over-reinforced (concrete crushing governs over FRP bar rupture). Note that $\rho_f > 1.4\rho_{fb}$, as recommended by the ACI 440 guide [28].

For an over-reinforced FRP-reinforced concrete beam, Whitney's rectangular stress block can be used to compute the nominal flexural capacity (M_n) in terms of the dimensions of the cross-section, FRP reinforcement ratio, stress in the FRP, and concrete compressive strength, as follows:

$$M_n = \rho_f f_f\left(1 - 0.59\frac{\rho_f f_f}{f'_c}\right) b\, d^2 \tag{4}$$

$$\begin{aligned} M_n &= 0.00473 * 750\left(1 - \tfrac{0.59 * 0.00473 * 750}{38.4}\right)(200)(239)^2 \\ &= 38.32 \times 10^6\ \text{N·mm} = 38.63\ \text{kN·m} \end{aligned}$$

in which f_f is the stress in the GFRP tensile reinforcement at ultimate, obtained from:

$$f_f = \sqrt{\frac{\left(E_f\varepsilon_{cu}\right)^2}{4} + \left(\frac{0.85\beta_1 f'_c}{\rho_f}\right)E_f\varepsilon_{cu}} - 0.5E_f\varepsilon_{cu} \tag{5}$$

$$f_f = \sqrt{\frac{(40,800 * 0.003)^2}{4} + \left(\frac{0.85 * 0.776 * 38.4}{0.00473}\right)(40,800 * 0.003)} - 0.5 * 40,800 * 0.003 = 750\ \text{MPa}$$

Note that in the above equation, the top steel was ignored since its contribution to the strength is negligibly small, as it is located within the tension zone just below the neutral axis (c = 33.5 mm < d' = 60 mm).

The computed flexural strength from theory, $M_n = 38.32$ kN·m, can be compared with the experimentally obtained values shown in Table 4 (34.04–39.93 kN·m) and corresponding averages provided in Table 5 (35.72–38.84 kN·m). The results of the comparison indicate that the ACI 440 [28] predictive equations for over-reinforced sections are reasonably accurate, especially when compared with the test results for the beams containing GFRP bars that were not subjected to harsh environmental conditions (Lab and Shade).

The theoretical cracking moment can be obtained by first computing the gross transformed moment of inertia of the section and then applying the flexure formula assuming linearly elastic behavior up to the point at which the bottom concrete fibers reach the tensile strength of the concrete. To do so, we first determine the location of the centroid of the section from the bottom after transforming the GFRP bars and steel bars to equivalent concrete:

$$\overline{y}_b = \frac{\sum A_i y_i}{\sum A_i} = \frac{A_c y_c + \left(n_f - 1\right)A_f y_f + (n_s - 1)A_s y_s}{A_c + \left(n_f - 1\right)A_f + (n_s - 1)A_s} \tag{6}$$

$$\overline{y}_b = \frac{200 * 300 * 150 + (1.40 - 1)226 * 61 + (6.87 - 1)157 * 240}{200 * 300 + (1.40 - 1)226 + (6.87 - 1)157} = 147.6 \text{ mm}$$

Since the modular ratios with respect to GFRP and steel, n_f and n_s, are given by:

$$n_f = {}^{E_f}/_{E_c} \text{ and } n_s = {}^{E_{fs}}/_{E_c} \tag{7}$$

$$=> n_f = \frac{E_f}{E_c} = \frac{E_f}{4700\sqrt{f'_c}} = \frac{40,800}{4700\sqrt{38.4}} = 1.40 \text{ and } n_s = \frac{E_s}{E_c} = \frac{E_s}{4700\sqrt{f'_c}} = \frac{200,000}{4700\sqrt{38.4}} = 6.87$$

where E_c is the modulus of elasticity of the concrete.

The corresponding gross moment of inertia, I_g, of the section about an axis passing through the centroid is

$$I_g = \sum \left(I_i + A_i {d_i}^2 \right) \tag{8}$$

$$\begin{aligned} I_g = \tfrac{200*300^3}{12} \quad & +200 * 300 \left(147.6 - \tfrac{300}{2}\right)^2 + (1 - 1.40)(226)(240 - 147.6)^2 \\ & +(1 - 6.87)(157)(240 - 147.6)^2 = 4.590 \times 10^8 \text{ mm}^4 \\ & = 4.590 \times 10^{-4} \text{ m}^4 \end{aligned}$$

The cracking moment is determined as the bending moment that is capable of imposing the modulus of rupture of the concrete, f_r, at the bottom fibers of the section:

$$\sigma = \frac{My}{I} \Longrightarrow M_{cr} = \frac{f_r I_g}{\overline{y}_b} \tag{9}$$

in which the modulus of rupture of the normal weight concrete is given by

$$f_r = 0.62\sqrt{f'_c} \tag{10}$$

$$M_{cr} = \frac{0.62\sqrt{38.4}\left(4.590 * 10^8\right)}{147.6} = 11.95 \times 10^6 \text{ N·mm}$$

The theoretically computed cracking moment, $M_{cr} = 11.95$ kN·m, can be compared with the experimentally found values shown in Table 4 (11.49–16.42 kN·m) and corresponding averages provided in Table 5 (12.88–14.95 kN·m). As expected, the predicted cracking moment represents a low estimate of the actual value because of the conservative modulus of rupture value of concrete recommended by the code and used in the equation. Figure 12 shows a graphical representation of the comparison between the experimental and theoretical moment capacities of all 10 considered beams in the study. Out of the 20 data points on cracking and ultimate flexural capacities, only 4 points related to the cracking moment are out of range. The remaining 16 data points demonstrate a good agreement between theory and experiments.

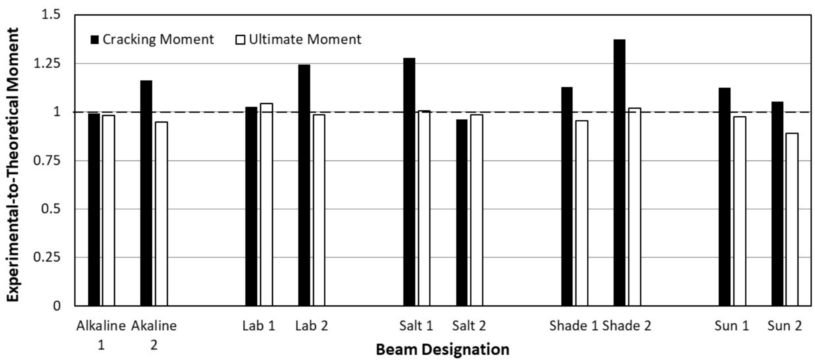

Figure 12. Normalized cracking and ultimate moment capacities of the tested beams.

The pre-cracking and post-cracking flexural stiffnesses of the tested beams can be estimated through calculations by considering the respective gross and effective second moment of area of the cross-section in the equation of the deflection as a function of the load effect, as shown in Figure 13.

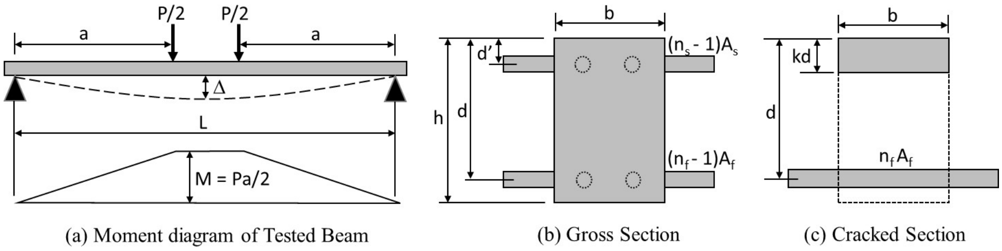

Figure 13. Moment diagram of tested beams and transformed cross-sections properties.

In order to predict the pre-cracking stiffness of the beam and compare it with the experimental values, we consider a simple beam of span L subjected to two downward concentrated loads, each of magnitude $P/2$, and located at distance a from the close support. From the theory of structures, one can obtain the equation of the midspan deflection, as follows:

$$\Delta = \frac{2\left(\frac{P}{2}\right)\left(\frac{L}{2}\right)\left[L^2 - (L-a)^2 - \left(\frac{L}{2}\right)^2\right]}{6E_c IL} \tag{11}$$

in which I is the transformed moment of inertia, in which the GFRP reinforcement is converted to concrete.

The above equation can be written in terms of the maximum moment, $M = Pa/L$, the modulus of elasticity of the concrete, and re-arranged so that the pre-cracking flexural stiffness, k_{pre}, can be determined from

$$k_{pre} = \frac{M}{\Delta} = \frac{6aE_c I_g}{(L-a)\left(2aL - a^2 - 0.25L^2\right)} \tag{12}$$

Substituting the values of a, f'_c, I_g, E_c, a, and L into the above expression using the units of kN and m, we obtain

$$k_{pre} = \frac{6(1.05)\left(4.7\times10^6\sqrt{38.4}\right)\left(4.590\times10^{-4}\right)}{(2.7-1.05)\left[2(1.05)(2.7) - (1.05)^2 - 0.25(2.7)^2\right]} = 18{,}595 \text{ kN}\cdot\text{m/m}$$

The above theoretical pre-cracking flexural stiffness can be compared with the experimentally determined values shown in Table 4 (11,692–19,724 kN·m/m) and corresponding averages provided in Table 5 (13,076–17,312 kN·m/m). For the most part, the estimated value compares reasonably well with the recorded ones from the laboratory tests.

To determine the post-cracking flexural stiffness, we consider the effective moment of inertia of the section after cracking occurs, as proposed by Bischoff [29] and adopted by the ACI 440 [28]:

$$I_e = \frac{I_{cr}}{1 - \gamma\left(\frac{M_{cr}}{M_a}\right)^2\left[1 - \left(\frac{I_{cr}}{I_g}\right)\right]} \le I_g \tag{13}$$

in which M_a is the maximum applied bending moment ion the beam (taken in this study as equal to 75% of the ultimate moment capacity, i.e., $M_a \approx 0.75M_n = 0.75 * 38.32 = 28.72$ kN·m), γ is a load and boundary conditions factor that accounts for the cracking pattern and change in stiffness along the beam, and I_{cr} is the moment of inertia of the cracked section. Due to its minimal impact on the calculations as a result of its location being close to the neutral axis, the compression steel on the top is ignored in the computation of the cracking moment.

$$\gamma = 1.72 - 0.72\left(\frac{M_{cr}}{M_a}\right) \tag{14}$$

$$\gamma = 1.72 - 0.72\left(\frac{11.95}{28.72}\right) = 1.42$$

and the cracked moment of inertia is given by:

$$I_{cr} = \frac{b(kd)^3}{3} + n_f A_f (d - kd)^2 \tag{15}$$

$$I_{cr} = \frac{200(25.97\ )^3}{3} + (1.40)(226)(239 - 25.97\ )^2 = 1.511 \times 10^7 \text{mm}^4 = 1.553 \times 10^{-5} \text{m}^4$$

in which kd is the depth of the flexural neutral axis from the top fibers when assuming the concrete stress to be proportional to strain, obtained from:

$$kd = \left[\sqrt{2n_f\rho_f + \left(n_f\rho_f\right)^2} - \left(n_f\rho_f\right)\right]d \tag{16}$$

$$kd = \left[\sqrt{2 * 1.40 * 0.00473 + (1.40 * 0.00473)^2} - (1.40 * 0.00473)\right](239) = 25.97\ \text{mm}$$

From the above values, the effective moment of inertia of the tested beams:

$$I_e = \frac{1.553 \times 10^{-5}}{1 - 1.40\left(\frac{11.95}{28.72}\right)^2 \left[1 - \left(\frac{1.553 \times 10^{-5}}{4.590 \times 10^{-4}}\right)\right]} = 2.028 \times 10^{-5}\ \text{m}^4$$

Using the above value of the effective moment of inertia instead of the gross moment of inertia in the previously considered equation of the deflection at midspan, Equation (12), we obtain the post-cracking stiffness, k_{post}:

$$k_{post} = \frac{M}{\Delta} = \frac{6aE_cI_e}{(L-a)\left(2aL - a^2 - 0.25L^2\right)} \tag{17}$$

$$k_{post} = \frac{6(1.05)\left(4.7 \times 10^6\sqrt{38.4}\right)\left(2.028 \times 10^{-5}\right)}{(2.7 - 1.05)\left[2(1.05)(2.7) - (1.05)^2 - 0.25(2.7)^2\right]} = 822\ \text{kN·m/m}$$

The above theoretical post-cracking stiffness can be compared with the experimentally determined values shown in Table 4 (508–593 kN·m/m) and corresponding averages provided in Table 5 (529–562 kN·m/m). It is clear from the comparison that the theory over-estimated the post-cracking stiffness. Note that that the post-cracking stiffness is highly unpredictable because it depends not only on the tensile strength of the concrete, but also the compressive stress–strain relation, cracking pattern along the beam, and crack propagation with the increase in the applied load. Further, the theoretical post-cracking stiffness formulation is greatly dependent on the assumed applied moment, which in the calculation was assumed to be 75% of ultimate moment capacity. Any value of the applied moment other than the assumed one would have impacted the magnitude of the post-cracking stiffness.

It should be noted that the theoretical analysis included in this section addresses the control beams that include intact GFRP reinforcement for the purpose of validating the experimental results of the reference case as a base of comparison. For those beams that contain degraded GFRP reinforcement due to exposure to outdoor weather, salt water, or alkaline solution, it is expected that the overall stiffness of the beam's cross-section will be impacted by the inferior stiffness of the exposed GFRP rebars. This will be reflected by a reduction in the gross and cracked-section properties.

5.3. Modelling of the Entire Flexural Response

Further examination of the shape of the experimentally obtained moment–deflection relationships of the GFRP-reinforced concrete beams considered in the study suggests that the envelope to the curve resembles that of the stress–strain curve of high-strength prestressing steel. Hence, it is believed that mathematical models available in the literature that have been used for simulating the behavior of prestressing steel in tension can be implemented for predicting the entire response of GFRP-reinforced beams if information about the cracking and ultimate conditions is known. One model that was proposed in 1979 by Mattock [30] seems to fit the experimental data at hand very well. The mathematical model consists of one equation that is characterized by three distinct parts, that starts with a nearly straight line having a steep slope, followed by a highly nonlinear part that transitions the first part to the third part which consists of an almost linear curve with a mild slope, as shown in Figure 14. By correlating the stress–strain material parameters at yield and ultimate by Mattock to the corresponding moment–deflection parameters in this study at cracking and ultimate, one can obtain the equation for the whole flexural $M - \Delta$ response of GFRP-reinforced beams under a four-point loading scheme.

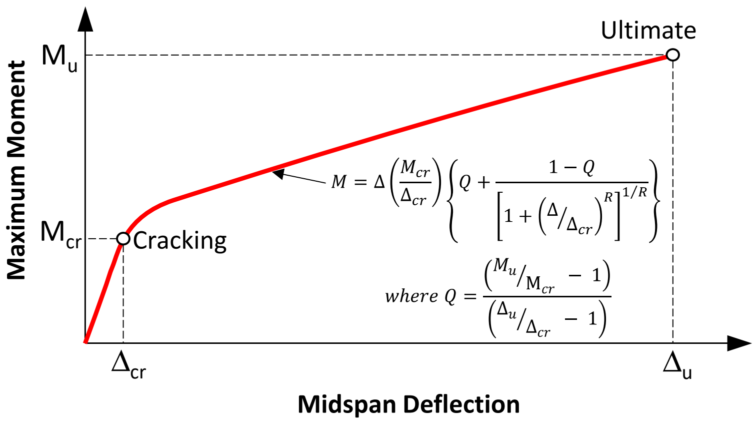

Figure 14. Modelling of the experimental flexural response by mathematical equation.

The equation of the full flexural $M - \Delta$ response, as a function of the moment capacity and associated deflection at initiation of cracking $(\Delta_{cr},\ M_{cr})$ and the moment capacity and associated deflection at ultimate $(\Delta_u,\ M_u)$, is given by

$$M = \Delta\left(\frac{M_{cr}}{\Delta_{cr}}\right)\left\{Q + \frac{1-Q}{\left[1+\left(\frac{\Delta}{\Delta_{cr}}\right)^R\right]^{1/R}}\right\} \tag{18}$$

in which Q is a constant that is related to the coordinates of the two most important points on the moment–deflection curve:

$$Q = \frac{\left(\frac{M_u}{M_{cr}} - 1\right)}{\left(\frac{\Delta_u}{\Delta_{cr}} - 1\right)} \tag{19}$$

In Equation (18), R is a constant that can be determined through a trial-and-error approach by solving the $M - \Delta$ equation for one of the two critical points at cracking or ultimate. In this study, R = 5 was found to give a reasonable prediction of the flexural behavior for all of the 10 tested beams. Figure 15 shows the experimental and corresponding theoretical $M - \Delta$ responses of two of the ten beams considered in the study, the beams Lab 2 and Sun 1. The proposed equation fits the other eight beams considered in the study equally well. Note that this proposed equation of the response is applicable to GFRP-reinforced concrete beams that are tested in flexure following a four-point loading scheme. Any deviations from this material and method of loading can render the proposed equation unapplicable.

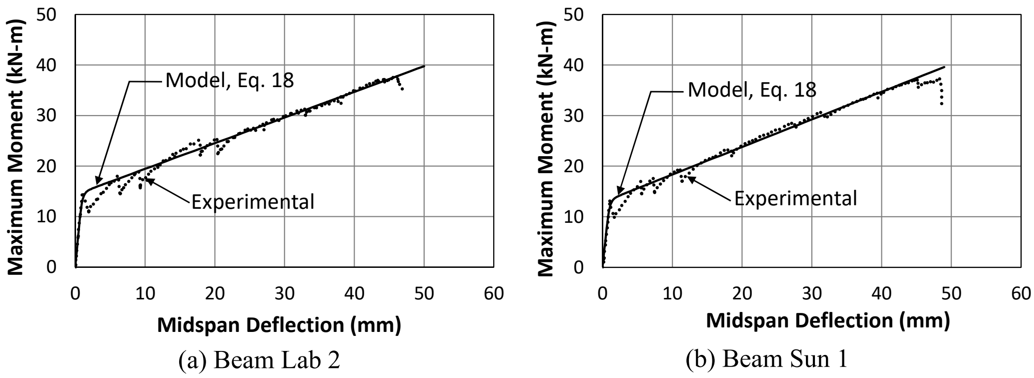

Figure 15. Comparison between the experimental and proposed model of the flexural response.

6. Conclusions

The findings of the study lead to the following conclusions:

1. Data from the strain gauges that were attached to the GFRP bars within the critical flexural region of the concrete beams confirmed the linear behavior of the embedded reinforcement with the increase in the applied load up to failure. No slippage due to bond failure between the surface of the GFRP bars and surrounding concrete was detected during the tests;
2. Crack width records from the tests indicated the superior serviceability of the beams that contained composite rebars that were stored in a controlled environment and the inferior serviceability of the beams that contained rebars that were stored outdoors for an extended period of time prior to using them as reinforcement in concrete;
3. The experimental test results showed that the moment capacity of the tested beams at ultimate was approximately 2.4–3.3 times the corresponding moment capacity at initial cracking, with the smallest ratios observed for the beams containing rebars that were exposed to an outdoor environment and the largest ratios for the control indoor beams. The flexural post-cracking stiffness was about 2.8–4.5% of the corresponding pre-cracking stiffness. The ductility index for the tested beams, measured as the deflection at ultimate to that at cracking, ranged between 2.9 and 4.16, with the higher value corresponding to one of the two control beams;
4. GFRP bar exposure to an alkaline solution or outdoor direct sunlight slightly affected the cracking and ultimate moment capacities, reducing them by, respectively, 5% and 3% from the same parameters of the controlled indoor exposure. While the influence of GFRP bar exposure on the post-cracking stiffness of beams was minimal, it had a great effect on the pre-cracking stiffness, resulting in about a 25% reduction for the outdoor shade and sun environments. The largest effect of bar exposure on flexural ductility was due to exposure to the outdoor climate, for which reductions of 20% and 10% were observed for bars subjected to open air shade and sun, respectively;
5. The predicted flexural strength at ultimate using the ACI 440 provisions gave comparable values when compared with the experimentally obtained results, with the difference between the two ranging between −4.2 to +12.6%. The cracking moment of the sections based on theoretical formulations was off the corresponding experimental findings by −4% to +28%;

6. While the computed pre-cracking flexural stiffness of the considered beams compared reasonably well with the experimentally obtained values, the computed post-cracking flexural stiffness over-estimated the experimental values by 28–38%;
7. A mathematical equation that envelopes the moment–deflection relationship for GFRP over-reinforced concrete beams is proposed. The equation requires information about two points on the curve, initial cracking and ultimate flexural conditions, and leads to close agreement with the experimental findings.

Author Contributions: Conceptualization, A.Z. and A.T.; methodology, S.W.T., A.Z. and A.T.; validation, S.W.T., A.T. and M.E.-E.; formal analysis, S.W.T.; resources, A.T.; writing—original draft preparation, S.W.T.; writing—review and editing, A.T. and M.E.-E.; supervision, A.T.; project administration, A.T.; funding acquisition, A.T. All authors have read and agreed to the published version of the manuscript.

Funding: The research was supported, in part, by the American University of Sharjah and the College of Engineering. The opinions included in the study are those of the authors and do not reflect the views of the funding agencies.

Institutional Review Board Statement: Not applicable.

Informed Consent Statement: Not applicable.

Data Availability Statement: All data are contained within the article.

Acknowledgments: Thanks are due to the engineers Arshi Faridi and Mohammad Ansari for supervising the experimental work in the structural laboratory at the American University of Sharjah. The authors are grateful to Farid Abed and Sherif Yehya for their feedback and contribution towards the experimental component of the study.

Conflicts of Interest: The authors declare no conflicts of interest. Author A.Z. was a graduate student at the American University of Sharjah at the time of this research and has since been employed by the company Qeyas Contracting L.L.C. The remaining authors declare that the research was conducted in the absence of any commercial or financial relationships that could be construed as a potential conflict of interest.

References

1. Li, S.; Lv, H.; Huang, T.; Zhang, Z.; Yao, J.; Ni, X. Degradation of Reinforced Concrete Beams Subjected to Sustained Loading and Multi-Environmental Factors. *Buildings* **2022**, *12*, 1382. [CrossRef]
2. Sbahieh, S.; Tahir, F.; Al-Ghamdi, S.G. Environmental and mechanical performance of different fiber reinforced polymers in beams. *Mater. Today Proc.* **2022**, *62*, 3548–3552. [CrossRef]
3. Ji, X.-L.; Chen, L.-J.; Liang, K.; Pan, W.; Su, R.K.-L. A review on FRP bars and supplementary cementitious materials for the next generation of sustainable and durable construction materials. *Constr. Build. Mater.* **2023**, *383*, 131403. [CrossRef]
4. Kinjawadekar, T.A.; Patil, S.; Nayak, G. A Critical Review on Glass Fiber-Reinforced Polymer Bars as Reinforcement in Flexural Members. *J. Inst. Eng. (India) Ser. A* **2023**, *104*, 501–516. [CrossRef]
5. Kim, H.-Y.; Park, Y.-H.; You, Y.-J.; Moon, C.-K. Short-term durability test for GFRP rods under various environmental conditions. *Compos. Struct.* **2008**, *83*, 37–47. [CrossRef]
6. Al-Salloum, Y.A.; El-Gamal, S.; Almusallam, T.; Alsayed, S.; Aqel, M. Effect of harsh environmental conditions on the tensile properties of GFRP bars. *Compos. Part B Eng.* **2012**, *45*, 835–844. [CrossRef]
7. El-Hassan, H.; El Maaddawy, T. Microstructure Characteristics of GFRP Reinforcing Bars in Harsh Environment. *Adv. Mater. Sci. Eng.* **2019**, *2019*, 8053843. [CrossRef]
8. Manalo, A.; Maranan, G.; Benmokrane, B.; Cousin, P.; Alajarmeh, O.; Ferdous, W.; Liang, R.; Hota, G. Comparative durability of GFRP composite reinforcing bars in concrete and in simulated concrete environments. *Cem. Concr. Compos.* **2020**, *109*, 103564. [CrossRef]
9. Vizentin, C.; Glujić, D.; Špada, V. Effect of time-real marine environment exposure on the mechanical behavior of FRP composites. *Sustainability* **2021**, *13*, 9934. [CrossRef]
10. Fergani, H.; Di Benedetti, M.; Oller, C.M.; Lynsdale, C.; Guadagnini, M. Durability and degradation mechanisms of GFRP reinforcement subjected to severe environments and sustained stress. *Constr. Build. Mater.* **2018**, *170*, 637–648. [CrossRef]
11. Davalos, J.F.; Chen, Y.; Ray, I. Long-term durability prediction models for GFRP bars in concrete environment. *J. Compos. Mater.* **2011**, *46*, 1899–1914. [CrossRef]
12. Gooranorimi, O.; Nanni, A. GFRP Reinforcement in Concrete after 15 Years of Service. *J. Compos. Constr.* **2017**, *21*, 04017024. [CrossRef]

13. Arczewska, P.; Polak, M.A.; Penlidis, A. Degradation of glass fiber reinforced polymer (GFRP) bars in concrete environment. *Constr. Build. Mater.* **2021**, *293*, 123451. [CrossRef]
14. Jin, Q.; Chen, P.; Gao, Y.; Du, A.; Liu, D.; Sun, L. Tensile Strength and Degradation of GFRP Bars under Combined Effects of Mechanical Load and Alkaline Solution. *Materials* **2020**, *13*, 3533. [CrossRef] [PubMed]
15. Al-Tamimia, A.; Abed, F.H.; Al-Rahmani, A. Effects of harsh environmental exposures on the bond capacity between concrete and GFRP reinforcing bars. *Adv. Concr. Constr.* **2014**, *2*, 1–11. [CrossRef]
16. Lu, C.; Yang, Y.; He, L. Mechanical and durability properties of GFRP bars exposed to aggressive solution environments. *Sci. Eng. Compos. Mater.* **2021**, *28*, 11–23. [CrossRef]
17. Maranan, G.; Manalo, A.; Benmokrane, B.; Karunasena, W.; Mendis, P. Evaluation of the flexural strength and serviceability of geopolymer concrete beams reinforced with glass-fibre-reinforced polymer (GFRP) bars. *Eng. Struct.* **2015**, *101*, 529–541. [CrossRef]
18. Nematzadeh, M.; Fallah-Valukolaee, S. Experimental and analytical investigation on structural behavior of two-layer fiber-reinforced concrete beams reinforced with steel and GFRP rebars. *Constr. Build. Mater.* **2021**, *273*, 121933. [CrossRef]
19. Abbas, H.; Abadel, A.; Almusallam, T.; Al-Salloum, Y. Experimental and analytical study of flexural performance of concrete beams reinforced with hybrid of GFRP and steel rebars. *Eng. Fail. Anal.* **2022**, *138*, 106397. [CrossRef]
20. Muhammad, M.A.; Ahmed, F.R. Evaluation of deflection and flexural performance of reinforced concrete beams with glass fiber reinforced polymer bars. *Case Stud. Constr. Mater.* **2023**, *18*, e01855. [CrossRef]
21. Mohammed, A.A.; Muhammad, M.A.; Mohammed, B.K. Effect of PET waste fiber addition on flexural behavior of concrete beams reinforced with GFRP bars. *Case Stud. Constr. Mater.* **2023**, *19*, e02564. [CrossRef]
22. Elangovan, G.; Rajanandhini, V. Flexural strength of Glass fiber reinforced polymer concrete beam with artificial Fine aggregate. *Mater. Today Proc.* **2022**, *62*, 1072–1077. [CrossRef]
23. Farias, C.; Pessi, S.; Wanderlind, A.; Piva, J.H.; Pavei, E. Flexural behavior of concrete beams reinforced with glass fiber reinforced polymer and steel bars. *Rev. De La Constr.* **2022**, *21*, 506–522. [CrossRef]
24. Ali, N.K.S.; Mahfouz, S.Y.; Amer, N.H. Flexural Response of Concrete Beams Reinforced with Steel and Fiber Reinforced Polymers. *Buildings* **2023**, *13*, 374. [CrossRef]
25. Gouda, O.; Asadian, A.; Galal, K. Flexural and Serviceability Behavior of Concrete Beams Reinforced with Ribbed GFRP Bars. *J. Compos. Constr.* **2022**, *26*, 04022064. [CrossRef]
26. Hassan, H.F.; Medhlom, M.K.; Ahmed, A.S.; Al-Dahlaki, M.H. Flexural performance of concrete beams reinforced by gfrp bars and strengthened by cfrp sheets. *Case Stud. Constr. Mater.* **2020**, *13*, e00417. [CrossRef]
27. Abed, F.; ElMesalami, N. Effect of Harsh Environmental Conditions on the Bond-Dependent Coefficient of GFRP Bars in Concrete Beams. In Proceedings of the 2019 Advances in Science and Engineering Technology International Conferences (ASET), Dubai, United Arab Emirates, 26–28 March 2019; pp. 1–5.
28. *ACI 440.1R-15*; ACI. Guide for the Design and Construction of Structural Concrete Reinforced with Fiber-Reinforced Polymer (FRP) Bars. American Concrete Institute: Detroit, MI, USA, 2021; 88p.
29. Bischoff, P.H. Reevaluation of Deflection Prediction for Concrete Beams Reinforced with Steel and Fiber Reinforced Polymer Bars. *J. Struct. Eng.* **2005**, *131*, 752–767. [CrossRef]
30. Mattock, A.H. Flexural Strength of Prestressed Concrete Sections by Programmable Calculator. *PCI J.* **1979**, *24*, 32–54. [CrossRef]